Research Article

Vol. 28, No. 4 / 17 February 2020 /

Optics EXPRESS

behavior which produces elastic distortions and topological defects, allowing for pre-defined nanoscale self-assembly of colloidal inclusions within the LC medium [11,15–18]. Moreover, the highly reconfigurable properties of LC materials can be controlled through external stimuli such as electric and magnetic fields, providing much-needed control over the optical interactions through the tunable inter-particle spacing between the nanoparticles.

In this work, we demonstrate how colloidal particles can self-assemble within the bulk of a

[redacted]

Optics EXPRESS

fluorescence signal from the QDs were collected by the same objective and recorded by an avalanche photodiode (APD) connected to a data acquisition board (NIDAQ-6363, National Instruments) and analyzed using a homebuilt MATLAB code. The fluorescence decay and photon antibunching characterization of the QDs fluorescence were performed using the same setup with slight modifications. For the fluorescence decay measurements, the QDs were excited using the 467 nm linearly polarized pulsed output from a diode laser (Nano LED- Horiba Scientific, 1 MHz, 200 ps) and the fluorescence signal detected by the APD was sent to a time-correlated single-photon counting hardware (TCSPC, SPC 130, Becker and Heckle) for further processing. Photon antibunching measurements were also performed under 473 nm linearly polarized CW laser excitation and the fluorescence signals from the QDs were analyzed using a Hanbury Brown-Twiss interferometer set-up. Within this setup, the fluorescence signal collected by the objective was split into two APDs using a 50/50 beam splitter and the coincidence counts between the photons arriving at the APDs were repeatedly measured with high temporal resolution, using the TCSPC hardware. The polarization state of the excitation beam was kept parallel to the far field director $\mathbf{n_0}$.

2.3. Numerical simulations

The simulations of electric field enhancement due to GMPs were performed using the COMSOL Multiphysics software. The pyramidal gold structures of GMPs were generated using the drawing tool in COMSOL, which were enclosed between perfectly matched layers on all sides to account for the boundary conditions. The simulations were performed assuming the standard refractive index values of gold and a constant refractive index value (= 1) for the medium. Due to computational limitations, the simulations for a single GMP were done for smaller particle size, with the base length of 2 µm, a factor of two smaller than what was used in experiments. For calculations involving four GMP assembly, the particle dimensions were reduced by a factor of 8. We then calculated the field intensity enhancement $\frac{|E|^2}{|E_0|^2}$ due to the GMPs at 620 nm, where E is the enhanced electric field component due to the GMPs and E_0 is the electric field component of the incident light.

3. Results and discussion

When dispersed in LC, the studied GMPs spontaneously orient with their base to apex vector **q** parallel to the far-field director $\mathbf{n_0}$, [19] as illustrated in Figs. 1(b)–1(e). In response to the tangential boundary conditions of the GMPs, the LC with the far-field director $\mathbf{n_0}$ becomes distorted near the GMPs, resulting in the localized director structures of **n(r)**, which are visible in the polarized microscopy images shown in Figs. 1(c) and 1(d). The spontaneous alignment of GMPs relative to $\mathbf{n_0}$ is a result of the minimization of free energy of the elastic distortions, which is achieved for the observed orientations of colloidal GMPs. The energy-minimizing director distortions around a GMP dispersed in LC are schematically represented in Fig. 1(e). The analysis of symmetry breaking indicates a dipolar elastic structure of the distortions around these particles [21]. The free energy minimization under these surface boundary conditions for the LC molecules create a topological defect called “boojums” very close to the apex of the pyramid, which is visible as a dark spot in the polarized optical microscopy images (Figs. 1(c) and 1(d)) and marked red in the schematic shown in Fig. 1(e). Owing to the minimization of elastic free energy cost, the small nanoparticles dispersed in the LC medium are attracted into boojums, being trapped by the elastic forces [22], providing an ideal platform for studying the optical interaction between the GMPs and a QD as illustrated below. The GMPs can be manipulated in the LC medium with the help of an optical trapping system by moving the focused laser beam of the laser tweezers. However, the control of particle orientation and movement by the laser tweezer is somewhat limited due to the melting of LC medium surrounding the GMPs

Optics EXPRESS

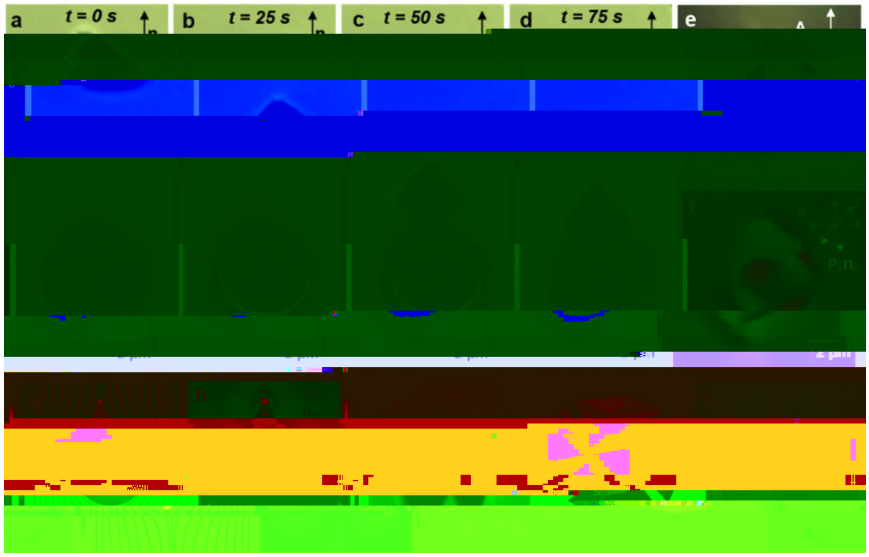

Fig. 2. Colloidal plasmonic superstructures fabricated through self-assembly. (a-d) Experimental sequence of optical micrographs, with elapsed time showing the assembly of a GMP and melamine resin sphere dispersed in LC. The final assembled colloidal structure is shown in (d). (e,f) Optical micrograph of the GMP-melamine sphere assembly obtained in polarized imaging mode without (e) and with (f) retardation plate. (g) Schematic representation of **n(r)** distortions around GMP-melamine resin sphere assembly showing far field director $\mathbf{n_0}$ and two boojums (marked in red). (h) Electric field intensity enhancement map around a GMP at 620 nm simulated using COMSOL Multiphysics. (i) Optical micrograph of the colloidal structure formed by the assembly of GMPs in LC obtained under brightfield microscopy. (j) Schematic representation of an idealized colloidal structure that

Optics EXPRESS

Fig. 3. Plasmonic e□ects on QD fluorescence. (a,b) Optical micrograph of a GMP dispersed in LC with a QD elastically trapped near the apex when viewed with a red filter under white light illumination (a) and with 473 nm excitation showing the fluorescence from QD (b). (c) Fluorescence decay curve from the QD located at the glass substrate (black square) of the confining cell and near the apex of a GMP dispersed in LC, representing typical fluorescence decay curves collected from two di□erent GMP-QD assemblies (green and blue triangles). Solid curves represent exponential fit to the experimental data.

The emission decay of the single QD fluorescence from the glass substrate follows a single exponential curve with a decay time 20 ns, which is the typical value of exciton lifetime for such a core-shell nanoparticle [4,28]. However, the fluorescence decay of the QD located at the apex of a GMP shows a double exponential decay, with average lifetimes $_1 = 2.5$ ns and $_2 = 8$ ns, indicating a three to 8 times enhancement in the radiative decay rates of the QD fluorescence, likely originating from the strong plasmon exciton interaction, due to the Purcell e□ect. The faster component in the QD fluorescence decay could arise from biexciton states of the QD emission owing to multiphoton absorption or from multiphoton emission as reported earlier [4]. Moreover, such observations are consistent for multiple GMP-QD assemblies (Fig. 3(c), compare the green and blue curves corresponding to di□erent GMP-QD pairs).

In order to analyze the multiphoton emission from the QD located at the apex of a GMP, we analyzed the QD emission using a photon antibunching set up. Figure 5 represents the typical photon antibunching curves of the emission for the QD on the glass substrate and at the apex of GMP. The data is fit using the expression $g^{(2)}(t) = g^{(2)}(0) + 1 \quad e^{-|t|/}$, where is the exciton lifetime, N is the number of photons and $g^{(2)}(0)$ is the second-order correlation at the coincidence time $t = 0$. For the data shown in Fig. 5(a), which corresponds to the QD fluorescence on glass substrate, we obtain $N = 1.1$, $g^{(2)}(0) = 0.15$ and $= 21$ ns. Similar analysis of the antibunching curve for the QD emission from the apex of GMP (Fig. 5(b)) yields $N = 1.23$, $g^{(2)}(0) = 0.25$, and $= 9$ ns. Both these results indicate single-photon emission property of the QDs, which also rules out the possible plasmon mediated multiphoton emission for the QD near the apex of GMP. However, the e□ect of plasmon exciton coupling is evident from the decreased exciton lifetime of the QD at the apex of the GMP extracted from the antibunching curve depicted in Fig. 5(b) as well as from the fluorescence decay curves (Fig. 3(c)). The observed variations in the optical

[redacted]

Optics EXPRESS

Fig. 5. Photon antibunching characterization of QD emission. Fluorescence antibunching curves of a single QD located at the surface of the glass substrate forming the LC cell (a) and elastically trapped near the apex of GMP dispersed in LC (b). Faster decay of the QD fluorescence is evident in (b) relative to (a), as revealed by the relatively sharper dip in the antibunching curve shown in (b). Solid lines represent fit to the experimental data.

Optics EXPRESS

medium by utilizing the elastic forces of interaction between them, which can be of interest to the study optical interaction at the nanoscale. While the use of plasmonic tips to probe the plasmon-exciton interactions is common, our work shows how such plasmonic tips can take the form of colloidal pyramids, which can be manipulated in a holonomic fashion by utilizing a combination of elasticity-mediated forces and laser trapping of high-index dielectric colloidal spheres co-self-assembled with these pyramids. Using this plasmonic enhancement tool, we have analyzed the optical properties of a single QD particle elastically trapped near the apex of a GMP using the time-resolved optical techniques and explained the results considering the plasmon exciton coupling. Since the elasticity-mediated colloidal interactions are long-ranged and extend to distances of about 10 μm [21,31], larger than all three types of used particles, one can envisage purely elastic hierarchical self-assembly based formation of desired colloidal superstructures. For example, one can envisage elasticity-mediated self-assembly of mesoscale crystals [31] formed by GMP-QD colloidal superstructures as building blocks, which would then lead to colloidal metamaterials with pre-designed properties stemming from the plasmon-exciton interactions. Moreover, elasticity-driven relative placement of plasmonic and semiconductor nanoparticles within LCs can be further enriched by additionally utilizing other known means, like DNA hybridization and origami-defined sca□olding that have been recently demonstrated in the nematic hosts as well [32]. Thus, the self-assembly method described here can be extended further and e□ectively used for the preparation of large-scale assemblies of metal and semiconductor

9. A. O. Govorov, G. W. Bryant, W. Zhang, T. Skeini, J. Lee, N. A. Kotov, J. M. Slocik, and R. R. Naik, "Exciton-plasmon interaction and hybrid excitons in semiconductor-metal nanoparticle assemblies," Nano Lett. **6**(5), 984–994 (2006).
10. T. Ozel, P. L. Hernandez-Martinez, E. Mutlugun, O. Akin, S. Nizamoglu, I. Ozge Ozel, Q. Zhang, Q. Xiong, and H. V. Demir, "Observation of selective plasmon-exciton coupling in nonradiative energy transfer: Donor-selective versus acceptor-selective," Nano Lett. **13**(7), 3065–3072 (2013).
11. P. Anger, P. Bharadwaj, and L. Novotny, "Enhancement and quenching of single-molecule fluorescence," Phys. Rev. Lett. **96**(11), 113002 (2006).
12. M. Haridas, J. K. Basu, D. J. Gosztola, and G. P. Wiederrecht, "Photoluminescence spectroscopy and lifetime measurements from self-assembled semiconductor-metal nanoparticle hybrid arrays," Appl. Phys. Lett. **97**(8), 083307 (2010).
13. Y. Ofir, B. Samanta, and V. M. Rotello, "Polymer and biopolymer mediated self-assembly of gold nanoparticles," Chem. Soc. Rev. **37**(9), 1814–1825 (2008).
14. S. Srivastava, D. Nykypanchuk, M. Fukuto, J. D. Halverson, A. V. Tkachenko, K. G. Yager, and O. Gang, "Two-dimensional DNA-programmable assembly of nanoparticles at liquid interfaces,"